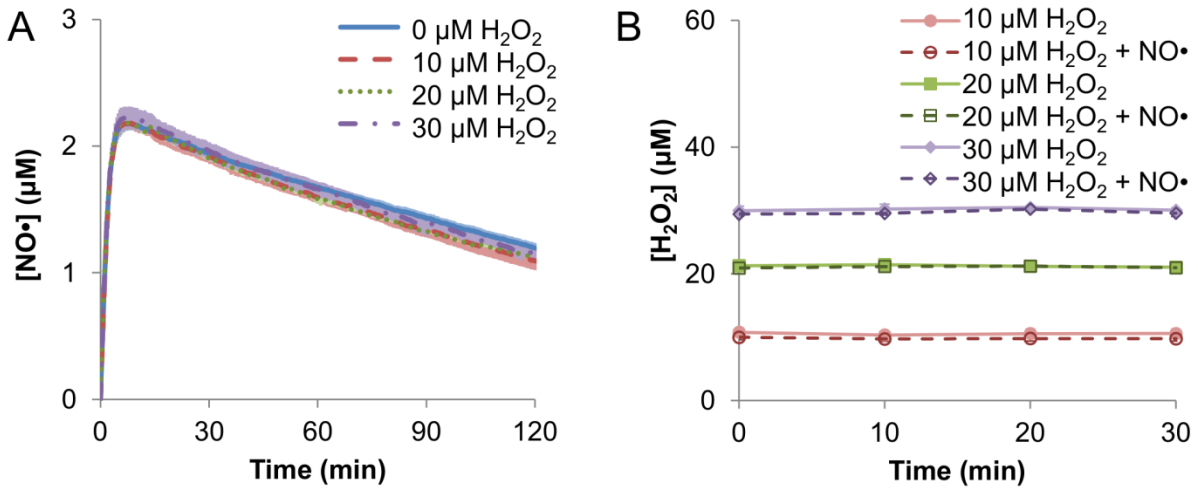

Fig. S1. Cell-free NO• and H_2O_2 controls. NO• (**A**) and H_2O_2 (**B**) consumption assays were performed in M9 media with 10 mM glucose lacking cells to account for any interactions between NO• and H_2O_2. The NO• curves did not differ in response to any H_2O_2 concentration, and H_2O_2 degradation was not affected in the presence of NO•. Darker lines (NO•) and solid dots (H_2O_2) are the means from at least three biological replicates, and the shaded regions around the darker lines and error bars show the standard error of the mean from those replicates.

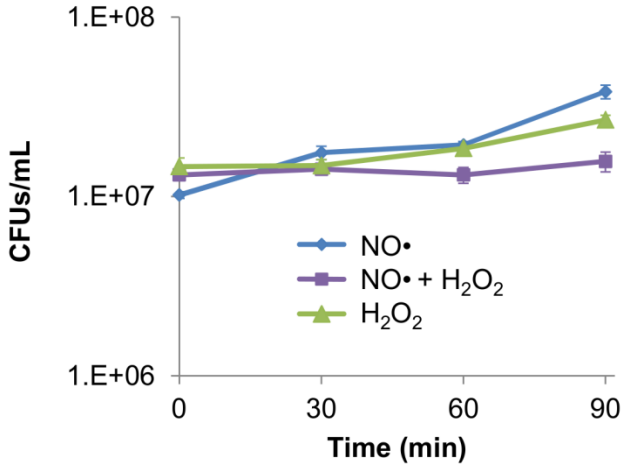

Fig. S2. Culturability during NO• and/or H_2O_2 treatment. Exponentially-growing cells were inoculated into a bioreactor containing M9 media with 10 mM glucose. At t=0, a sample was taken prior to the addition of 0 or 30 µM H_2O_2, followed by 50 µM DPTA or an equivalent amount of the DPTA solvent. Under no condition was there a significant decrease in CFUs/mL. Data represents the average of at least three biological replicates, with error bars showing the standard error of the mean.

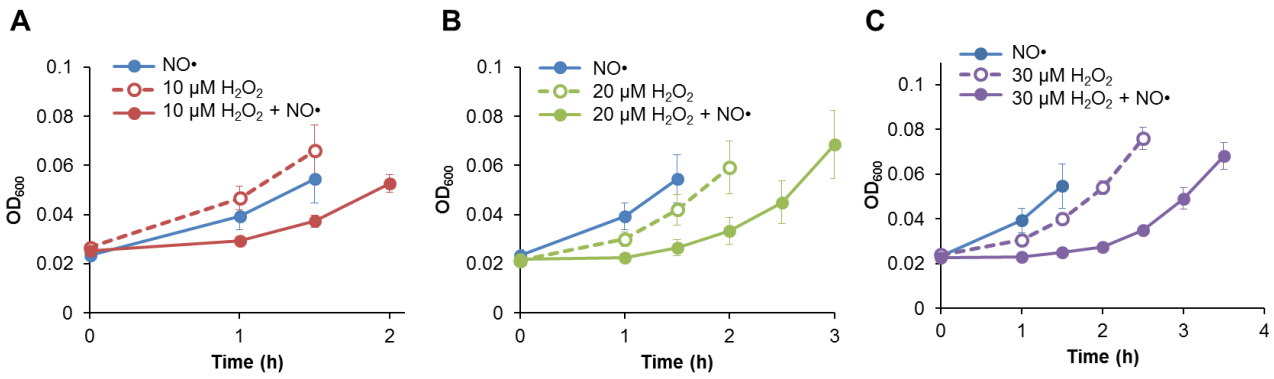

Fig. S3. Re-growth following NO• and/or H_2O_2 treatment. OD_{600} was monitored following treatment with 50 μM DPTA and/or H_2O_2. All samples resumed growth following treatment, after the clearance of both NO• and H_2O_2. Data represents the average of at least three biological replicates, with error bars showing the standard error of the mean.

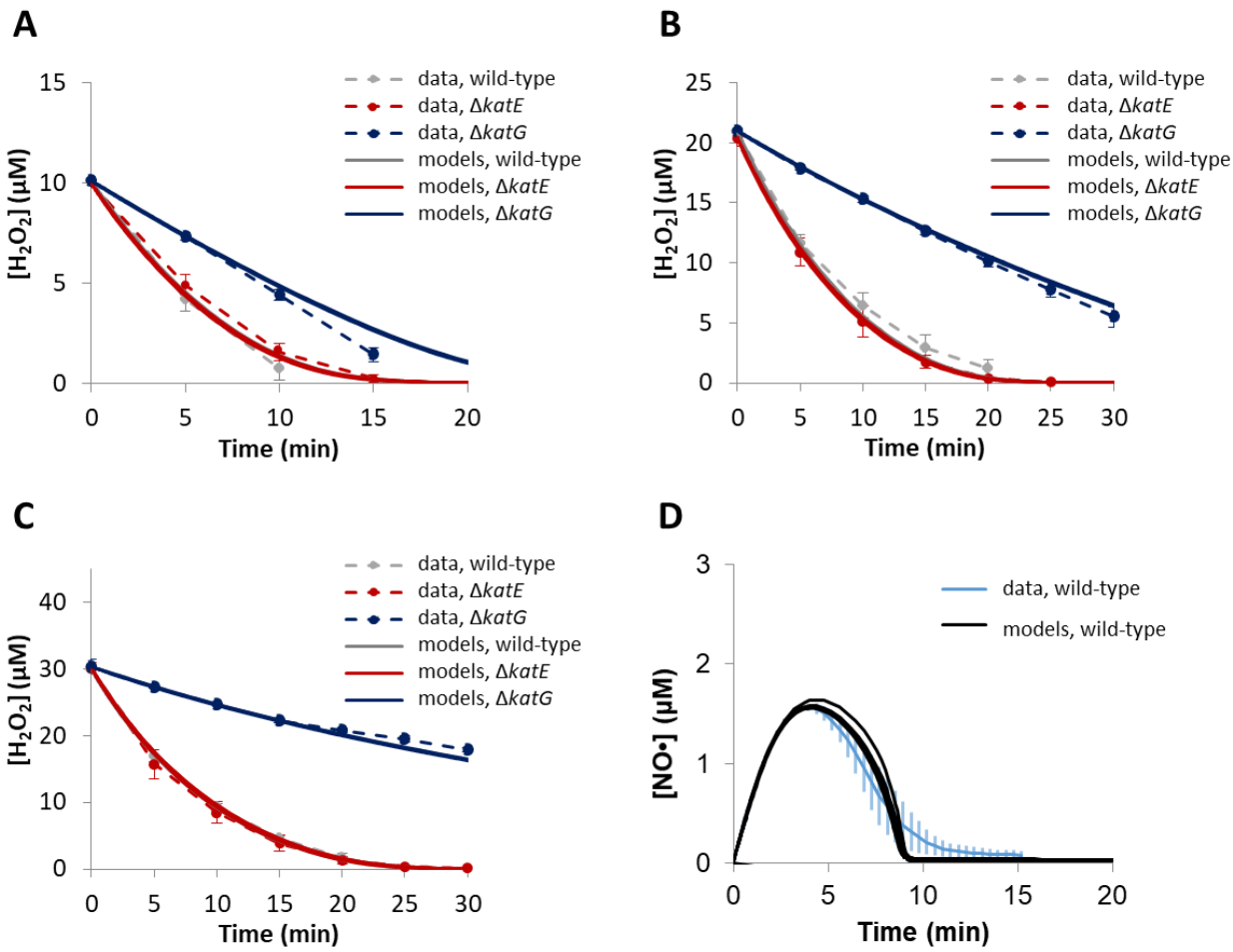

Fig. S4. Simulation and experimental results under various H_2O_2 and NO• stress conditions. Simulated and observed H_2O_2 clearance profiles of wild-type, Δ*katE*, and Δ*katG* when 10 μM H_2O_2 (A), 20 μM H_2O_2 (B) or 30 μM H_2O_2 (C) was added at t = 0 min. (D) Simulated and observed wild-type NO• clearance profiles after treatment of 50 μM DPTA at t = 0 min. For simulation data, all models with ER < 10 were used to predict cellular responses. For experimental data, the solid lines and solid dots are the means from at least three biological replicates, and the shaded regions around the solid lines and error bars show the standard error of the mean from those replicates.

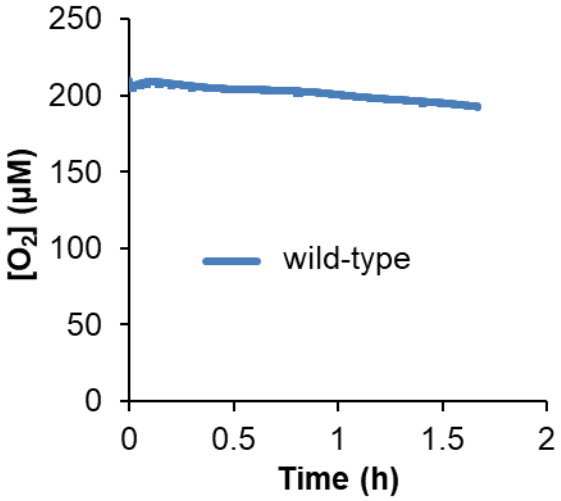

Fig. S5. Oxygen concentration in the bioreactor following NO• and H_2O_2 treatment.

Exponentially-growing wild-type cells were treated with 30 µM H_2O_2 and 50 µM DPTA in the bioreactor. O_2 concentration in the bioreactor was continuously monitored using an O_2 probe. The solid line represents the averages of three biological replicates, with shaded regions around the solid line showing the standard error of the mean.

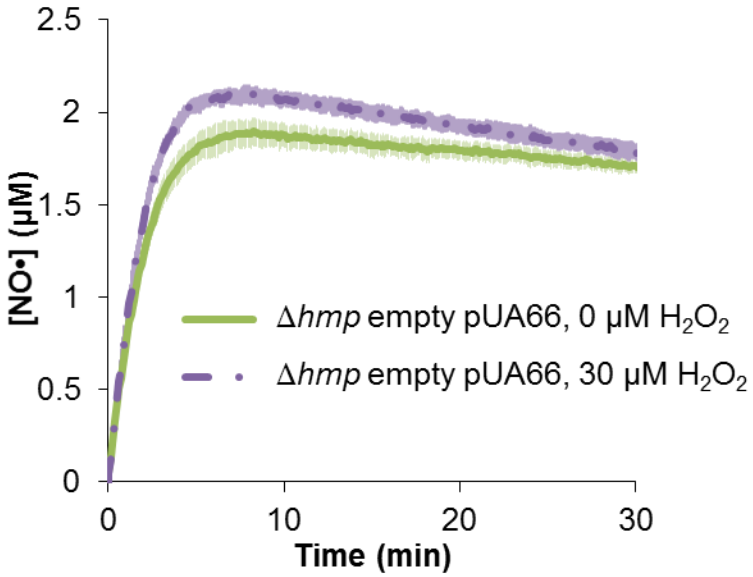

Fig. S6. **pUA66 did not affect the phenotype of Δ*hmp*.** The inclusion of an empty pUA66 plasmid did not alter the NO• detoxifying capability of Δ*hmp*. Detoxification of NO• was still not observed, regardless of the presence of H_2O_2. The darker lines represent the means of 3 independent replicates, and the shaded regions around the darker lines the standard errors of the means.

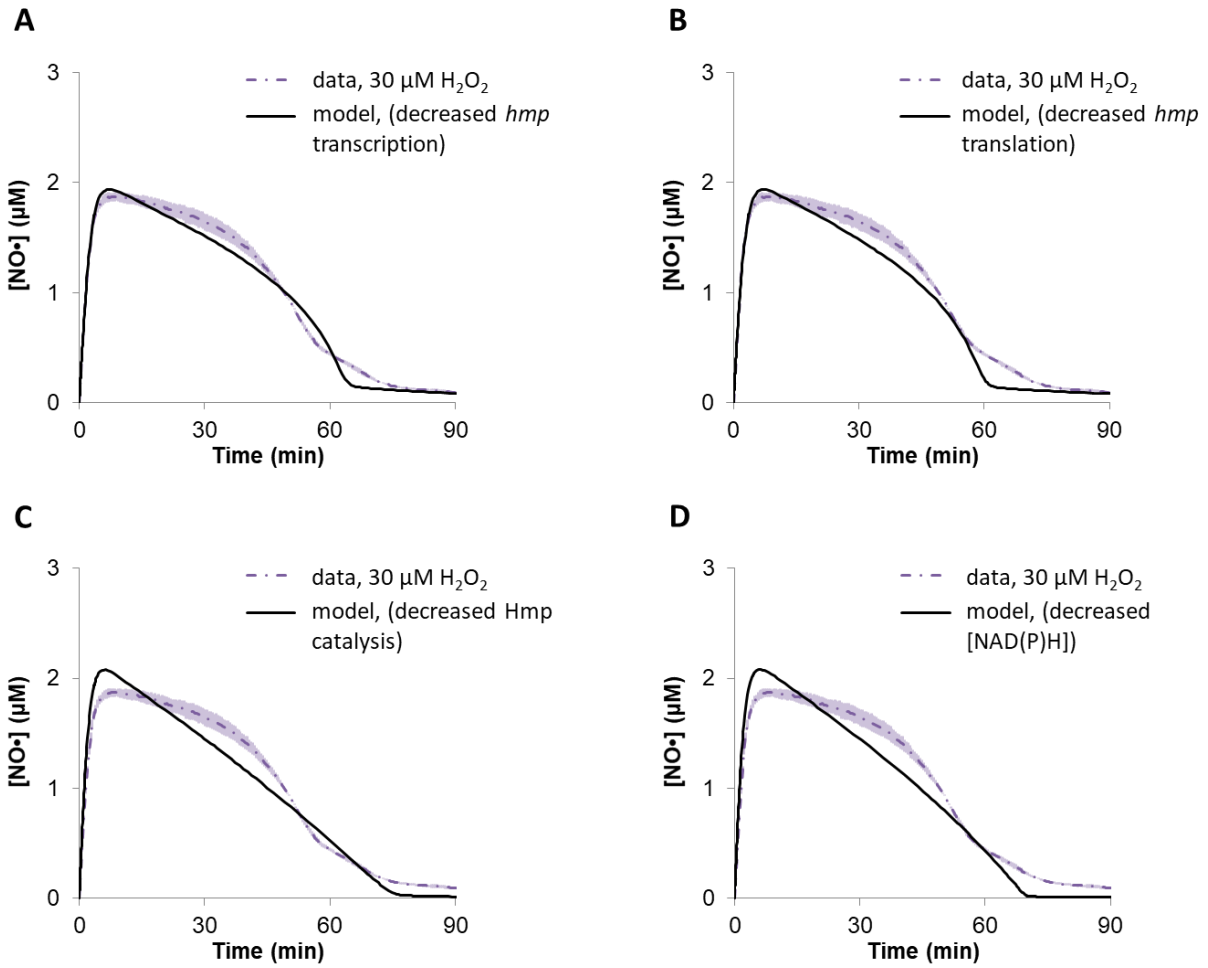

Fig. S7. Simulations depict modes of how H_2O_2 could interfere with NO• detoxification.

Parameters in the best fit model were individually altered to capture the delay in NO• clearance under concurrent exposure to NO• and H_2O_2. The rate of *hmp* transcription (*p_HMPtranscr_kmax*) was reduced in (A), the rate of Hmp translation (*p_HMPtranslate_k*) was decreased in (B), the catalytic activity of Hmp (*p_HMP_kP*) was reduced in (C), and the concentrations of NADPH and NADH were dropped in (D). The dashed line show the averages of three independent replicates, and the shaded region around the dashed line represents the standard error of the mean.

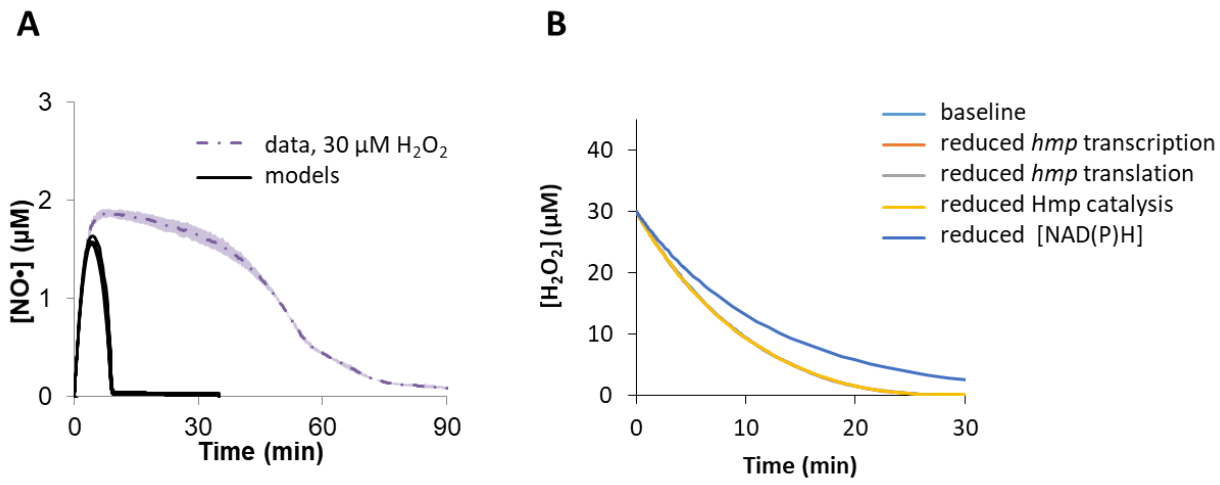

Fig. S8. **Simulation results under simultaneous stress.** (A) The ensemble of models was not able to capture the delay in NO• clearance driven by the concurrent treatment of 30 µM H_2O_2. For the experimental data, the dashed line shows the average of 3 biological replicates, and the shading the accompanying standard errors. (B) The alterations of parameter values in the best-fit model that were able to recapitulate NO• data from co-treatment conditions (Fig. S7). Here, the predictions of H_2O_2 clearance by those models are plotted. Notably, the decrease in [NAD(P)H] resulted in a delayed H_2O_2 clearance, which is inconsistent with observed experimental data.

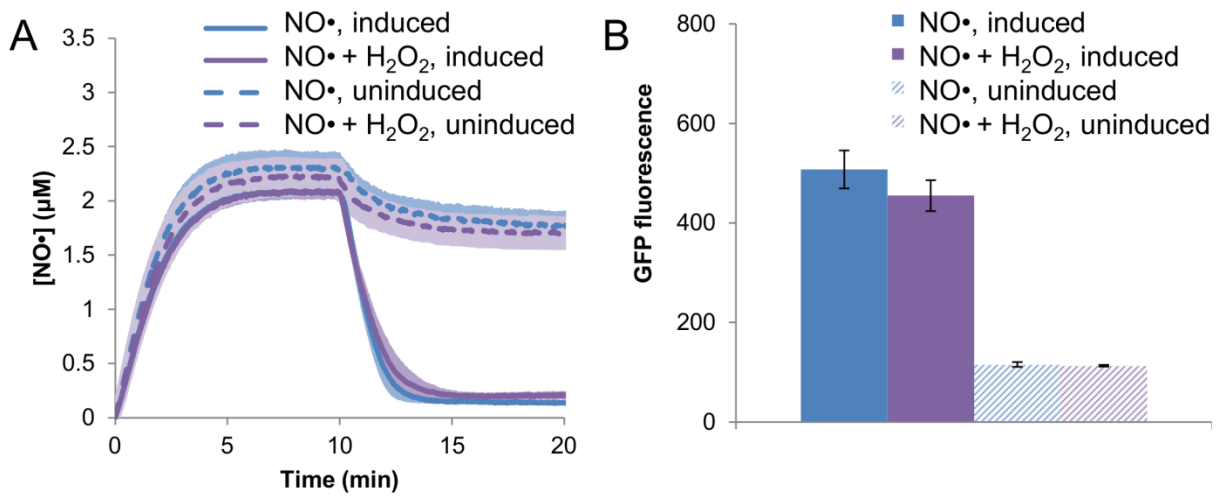

Fig. S9. Uninduced controls for catalytic activity assay. To account for leak from the plasmid, the experiment shown in Fig. 5 was repeated without inducer. The background expression level allows for a minimal amount of NO• detoxification (**A**). Dashed lines show the uninduced controls, whereas solid lines show the induced samples (from Fig. 5) and are included for reference. GFP levels associated with induced (solid bars) and uninduced (dashed bars) are shown in (**B**). Both panels show the average of three biological replicates, where error bars represent the standard error of the mean.

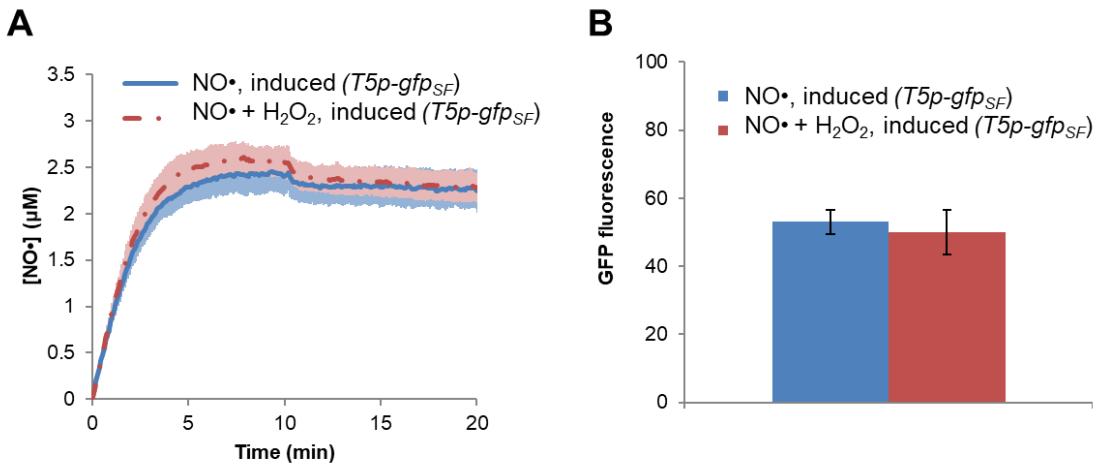

Fig. S10. Induced controls for catalytic activity assay. To account for presence of GFP_{SF} and IPTG, the experiment shown in Fig. 5 was repeated by inducing the expression GFP_{SF} from the same inducible promoter with the same concentration of IPTG, in a Δ*hmp* strain. The difference between the plasmid used here and that used in Fig. 5 is the absence of *hmp*; the one here expresses GFP whereas that portrayed in Fig. 5 and S9 express an Φ(Hmp-GFP) translational fusion protein. NO· clearance capability of this strain was unaffected by the presence of H_2O_2. GFP levels are shown in (**B**). Both panels show the average of three biological replicates, where error bars represent the standard error of the mean.

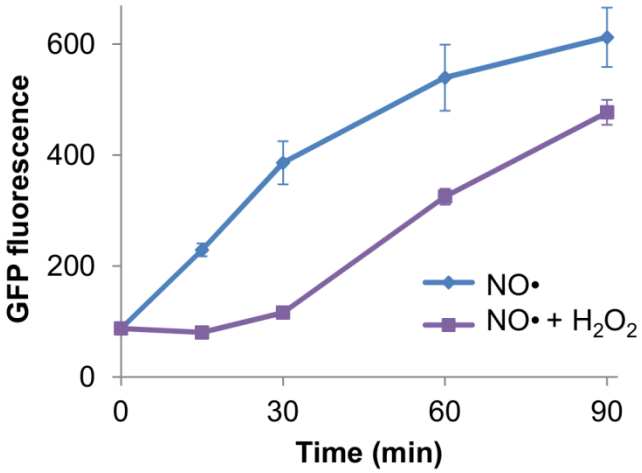

Fig. S11. Expression from *hmp* promoter is regained after H_2O_2 clearance. At longer time scales than those shown in Fig. 6 (t=60 and 90 min), measurable GFP synthesis under the control of the *hmp* promoter is observed. H_2O_2 is cleared at ~25 min. Time 0, 15 min, and 30 min (from Fig. 6) are shown for reference.

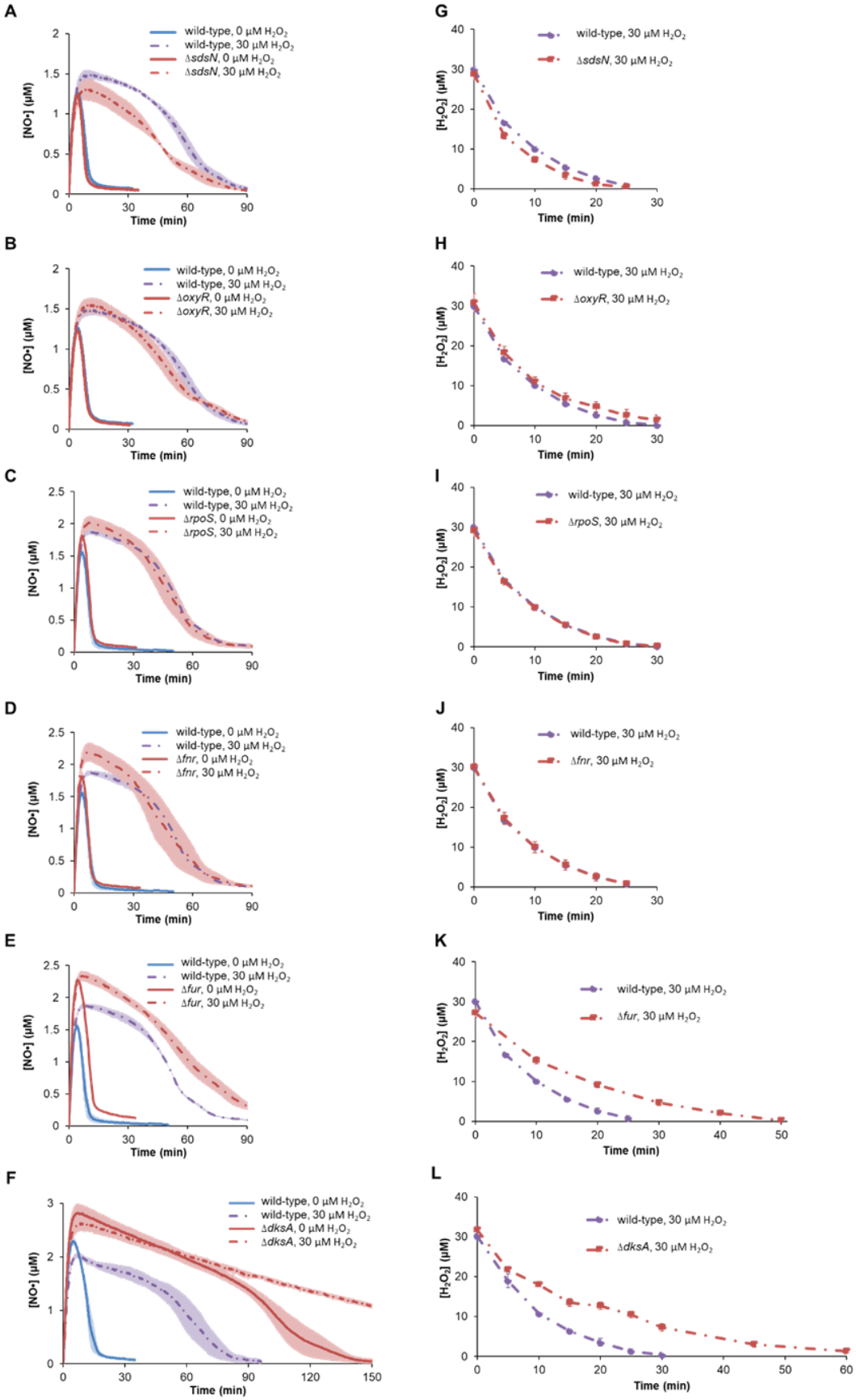
A
wild-type, 0 μM H2O2
wild-type, 30 μM H2O2
ΔsdsN, 0 μM H2O2
ΔsdsN, 30 μM H2O2
[NO•] (μM)
Time (min)
G
wild-type, 30 μM H2O2
ΔsdsN, 30 μM H2O2
[H2O2] (μM)
Time (min)
B
wild-type, 0 μM H2O2
wild-type, 30 μM H2O2
ΔoxyR, 0 μM H2O2
ΔoxyR, 30 μM H2O2
[NO•] (μM)
Time (min)
H
wild-type, 30 μM H2O2
ΔoxyR, 30 μM H2O2
[H2O2] (μM)
Time (min)
C
wild-type, 0 μM H2O2
wild-type, 30 μM H2O2
ΔrpoS, 0 μM H2O2
ΔrpoS, 30 μM H2O2
[NO•] (μM)
Time (min)
I
wild-type, 30 μM H2O2
ΔrpoS, 30 μM H2O2
[H2O2] (μM)
Time (min)
D
wild-type, 0 μM H2O2
wild-type, 30 μM H2O2
Δfnr, 0 μM H2O2
Δfnr, 30 μM H2O2
[NO•] (μM)
Time (min)
J
wild-type, 30 μM H2O2
Δfnr, 30 μM H2O2
[H2O2] (μM)
Time (min)
E
wild-type, 0 μM H2O2
wild-type, 30 μM H2O2
Δfur, 0 μM H2O2
Δfur, 30 μM H2O2
[NO•] (μM)
Time (min)
K
wild-type, 30 μM H2O2
Δfur, 30 μM H2O2
[H2O2] (μM)
Time (min)
F
wild-type, 0 μM H2O2
wild-type, 30 μM H2O2
ΔdksA, 0 μM H2O2
ΔdksA, 30 μM H2O2
[NO•] (μM)
Time (min)
L
wild-type, 30 μM H2O2
ΔdksA, 30 μM H2O2
[H2O2] (μM)
Time (min)

Fig. S12. NO• and H_2O_2 clearance profiles in mutants known to influence *hmp* and/or *katG* transcription. Exponentially-growing Δ*sdsN*, Δ*oxyR*, Δ*rpoS*, Δ*fnr*, Δ*fur*, and Δ*dksA* cells were inoculated into a bioreactor containing 0 or 30 μM H_2O_2 in the bioreactor. The culture was then immediately treated with 50 μM DPTA. NO• (**A-F**) was monitored continuously, whereas H_2O_2 concentration (**G-L**) was quantified every 5 min, 10 min or 15 min depending on the clearance time of H_2O_2. In **F** and **L**, because Δ*dksA* requires amino acid supplementation, wild-type was grown and stressed in M9 minAA to maintain consistency. Error bars show the standard error of the mean from three biological replicates.

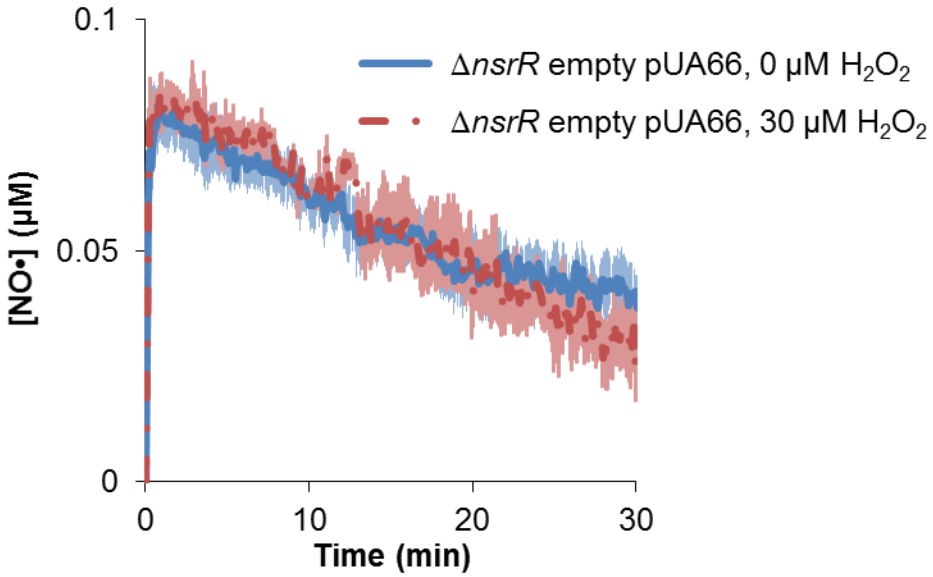

Fig. S13. **pUA66 did not affect the phenotype of Δ*nsrR*.** The inclusion of an empty pUA66 plasmid did not alter the NO• detoxifying capability of Δ*nsrR*. There was simultaneous clearance of NO• by cells regardless of the presence of H_2O_2, potentially due to constitutive expression of *hmp* in the absence of a functional NsrR. The darker lines represent the means of three independent replicates, and the shaded regions around the darker lines the standard errors of the means.

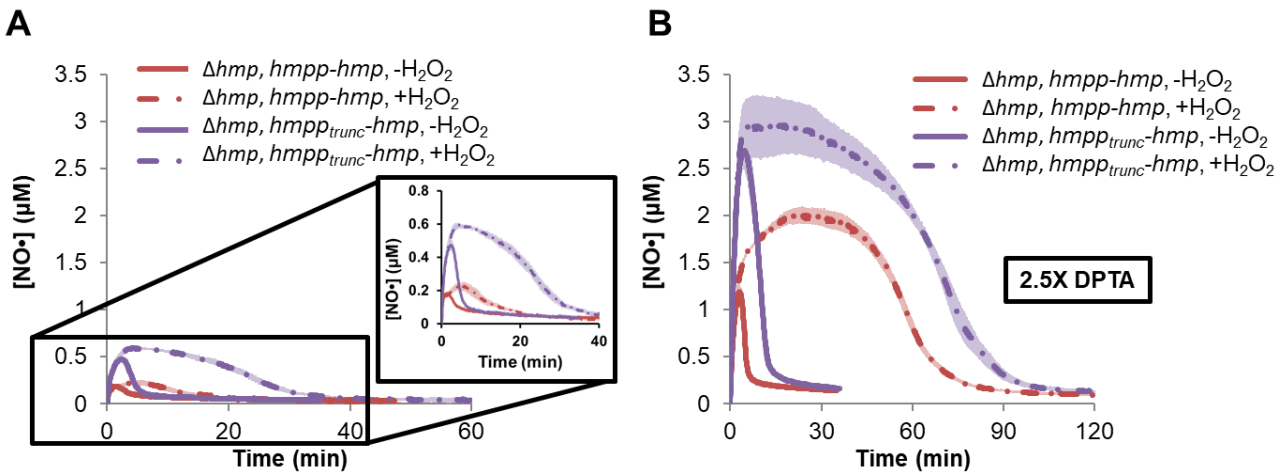

Fig. S14. MetR binding site in *hmp* promoter is important for activation of expression. On the *hmp* expression plasmids, MetR binding sites were either included or excluded (*hmpp*$_{trunc}$) from the promoter. In the absence of MetR binding sites, H_2O_2 still delayed NO• detoxification. Due to copy number or leakiness effects from the plasmid-borne *hmp*, cells could more readily consume NO• when 50 μM DPTA was delivered, resulting in a comparatively low [NO•] peak and fast NO• clearance (A). When the concentration of DPTA was increased 2.5 fold to 125 μM, the NO• concentration was closer to what was observed in wild-type cultures. The solid and dashed lines represent the averages of three independent replicates, and the shading around those lines indicates the standard errors of those means.

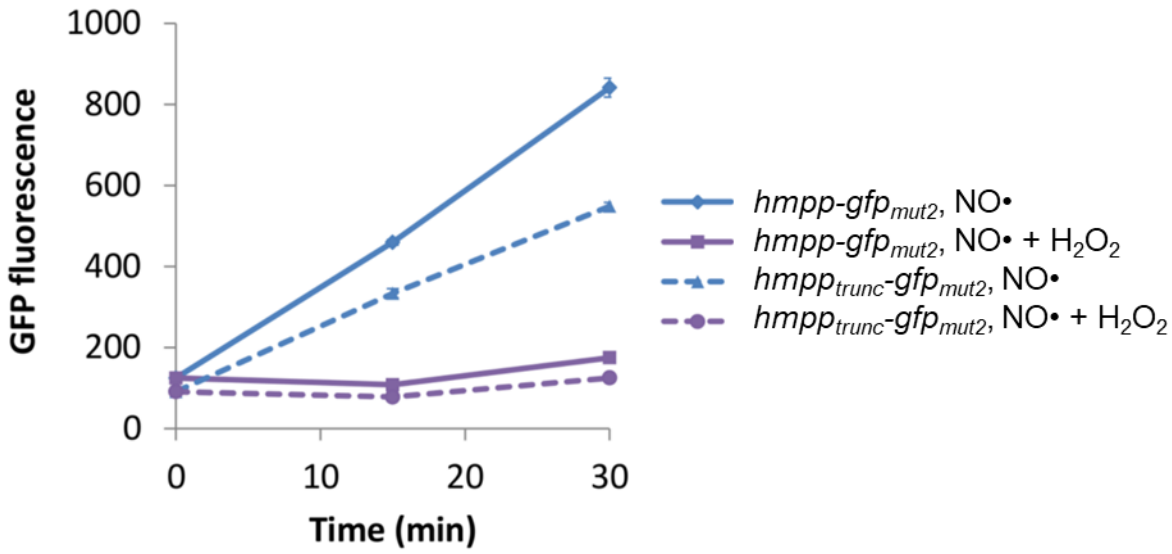

Fig. S15. MetR is not responsible for H_2O_2-dependent suppression of *hmp* induction.

Exponentially-growing Δ*hmp* cells transformed with an *hmp* transcriptional reporter (pUA66 *hmpp-gfp*$_{mut2}$), or an analogous reporter truncated to remove the *metR* binding site (pUA66 *hmpp*$_{trunc}$*-gfp*$_{mut2}$) were inoculated into a bioreactor containing 0 or 30 µM H_2O_2 in M9 media with 10 mM glucose, then immediately treated with 50 µM DPTA. A Δ*hmp* background was used to maintain identical NO• environments in the two samples. Transcription is significantly inhibited ($p<0.05$ at 15 and 30 min) in the presence of H_2O_2 regardless of whether the *metR* binding site is present. However, maximal induction of transcription appears to require the *metR* site. Error bars show the standard error of the mean from three biological replicates. The asterisk (*) represents significant difference while comparing solid to solid, and dashed to dashed lines.

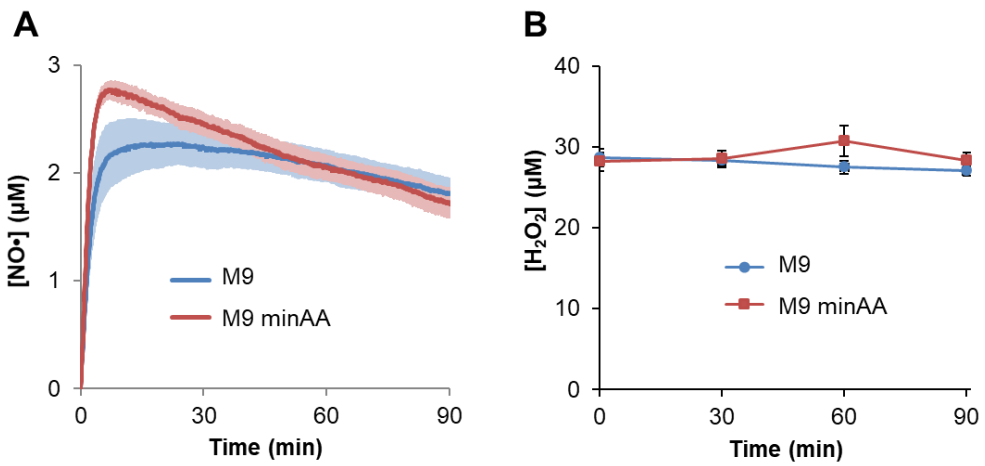

Fig. S16. MinAA supplement does not affect dynamics of NO• and H_2O_2. 50 μM DPTA (A) or 30 μM H_2O_2 (B) was added to cell-free M9 media with 10 mM glucose (M9) or that media with minAA (M9 minAA). The inclusion of minAA in the media does not seem to cause significant changes to the dynamics of NO• and stability of H_2O_2. The solid lines and dots represent the averages from three independent replicates, and the shading and error bars the standard errors of those means.

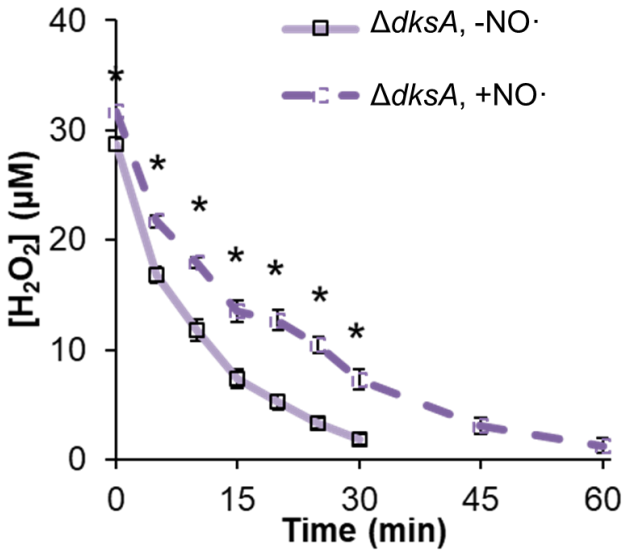

Fig. S17. NO• delays H_2O_2 clearance in Δ*dksA*. Exponentially-growing Δ*dksA* was transferred to a bioreactor containing M9 media with 10 mM glucose and 30 μM H_2O_2. Cells were then treated with either 0 or 50 μM DPTA. The presence of NO• delays H_2O_2 clearance in Δ*dksA* by about 2-fold. The data points are the means of at least three biological replicates, and the error bars represent the standard errors. The asterisk (*) illustrates a significant difference between H_2O_2 concentrations at the same time point for with and without NO• samples using a p-value threshold < 0.05.

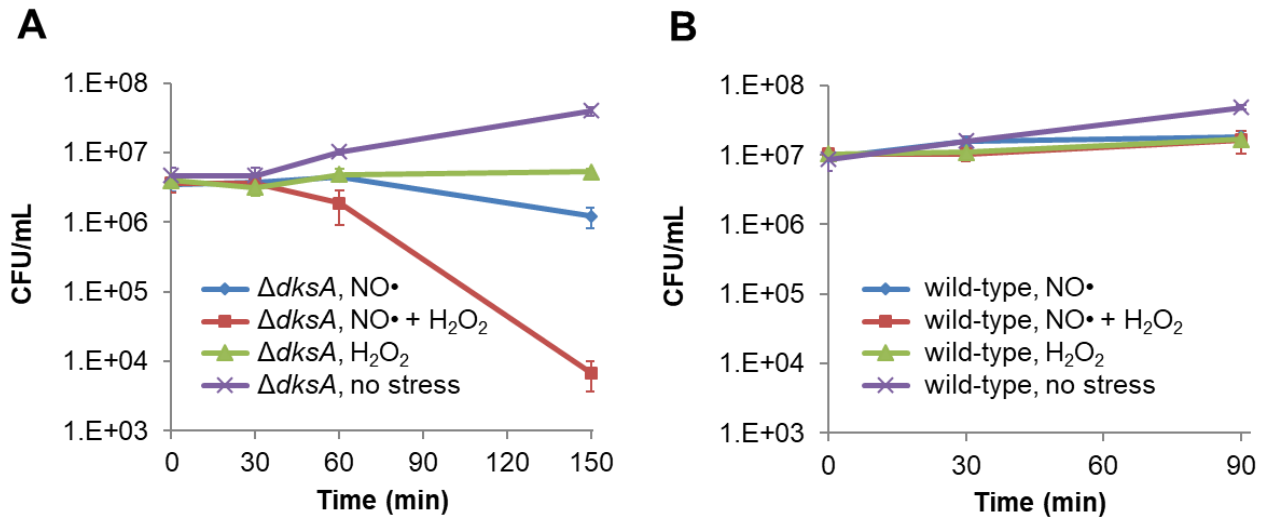

Fig. S18. NO• causes cell death in Δ*dksA*. Δ*dksA* and wild-type were grown to OD_{600} ~ 0.2 in M9 minAA. Exponentially-growing cells were then inoculated into a bioreactor containing M9 minAA. Before H_2O_2 and DPTA treatments, 200 µL of culture was removed and plated on LB agar for CFU enumeration. Afterward, 0 or 30 µM H_2O_2 and 50 µM DPTA or the same volume of solvent (10 mM NaOH) were added. 200 µL of the content in bioreactor was withdrawn at indicated times following treatment and plated on LB agar overnight. The data points represent the means of 3 independent replicates, and the error bars the standard errors of those means.

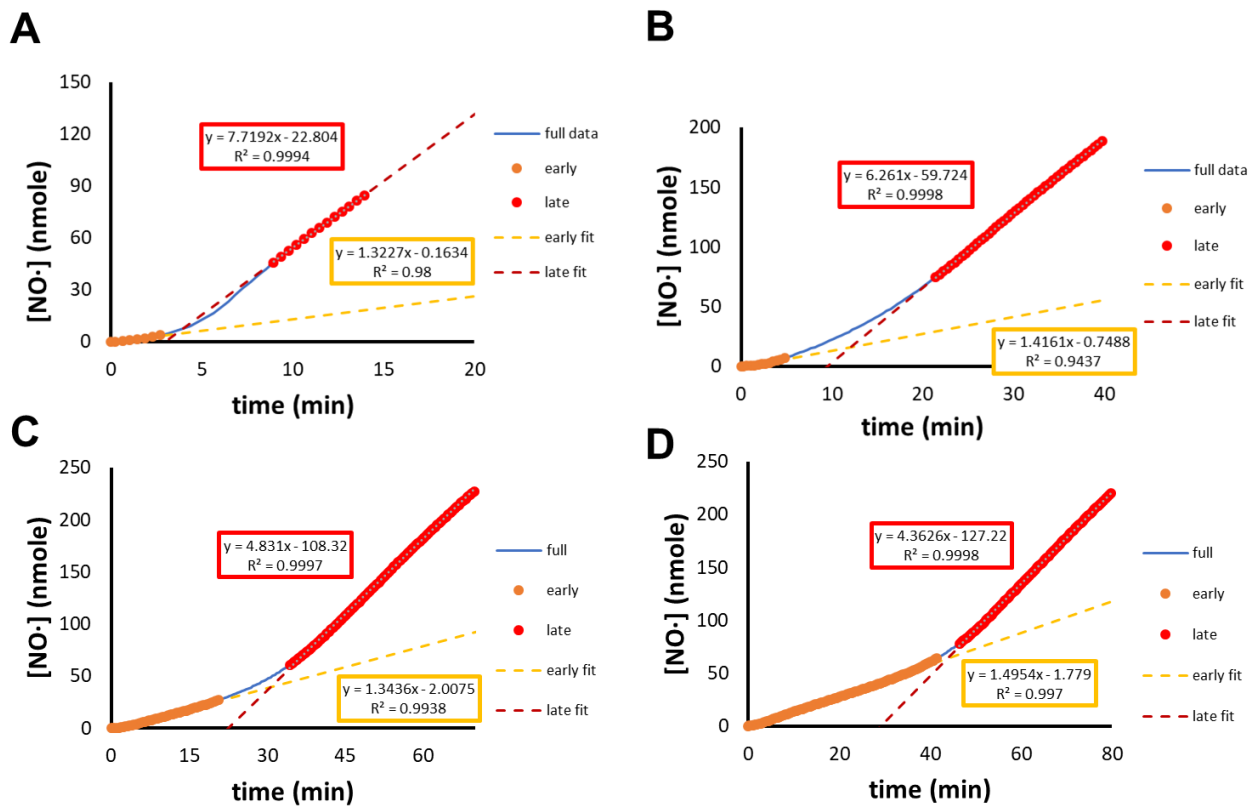

Fig. S19. Linear fits of different regimes of NO· consumption. The rates of NO· consumption under different H_2O_2 conditions (0 μM (A),10 μM (B), 20 μM (C), and 30 μM (D)) were approximated by the slopes of the linear fits for different regimes. The equation and R^2 of each fit are presented in the box of the corresponding color.

Table S1. Bacterial strain and plasmid table. Bacterial strains and plasmids used in this study.

Strain	Genotype	Reference
MG1655	wild-type	[1]
WCKA01	MG1655 Δ*nsrR*::*kan*	This work
WCKA02	MG1655 Δ*nsrR*::*scar*	This work
WCKA03	MG1655 Δ*hmp*::*kan*	This work
WCKA04	MG1655 Δ*hmp*::*scar*	This work
WCKA05	MG1655 Δ*katE*::*kan*	This work
WCKA06	MG1655 Δ*katG*::*kan*	This work
WCKA07	MG1655 Δ*sdsN*::*kan*	This work
WCKA08	MG1655 Δ*oxyR*::*kan*	This work
WCKA09	MG1655 Δ*rpoS*::*kan*	This work
WCKA10	MG1655 Δ*fur*::*kan*	This work
WCKA11	MG1655 Δ*fnr*::*kan*	This work
WCKA12	MG1655 Δ*dksA*::*kan*	[2]
Plasmid	**Genotype**	**Source or Reference**
pUA66	Vector, SC101ori, *kan*, *gfpmut2* reporter	[3]
pCP20	Vector, *amp, flp*	[4]
pKD46	Vector, *amp, araC, araBp-exo-bet-gam*	[5]
pKD4	Vector, *kan, amp*	[5]
pWCKA01	pUA66 *T5p*-Φ(*hmp-gfp*$_{SF}$), *lacI*^{q}	[6]
pWCKA02	pUA66 *hmpp-hmp*	This work
pWCKA03	pUA66 *hmpp*$_{trunc}$*-hmp* (- MetR binding sites)	This work
pWCKA04	pUA66 *nsrRp-nsrR*	This work
pWCKA05	pUA66 *hmpp-gfp*$_{mut2}$	This work
pWCKA06	pUA66 *hmpp*$_{trunc}$*-gfp*$_{mut2}$	This work
pWCKA07	pUA66 *katGp-gfp*$_{mut2}$	This work
pWCKA08	pUA66 *T5p-gfp*$_{SF}$, *lacI*^{q}	[5]
pWCKA09	pET-11a-*phzM*	[5]

Table S2.1: PCR check primers

Deletion	Forward external primer[a,c]	Reverse external primer[c]	Forward internal primer[b]	Reverse internal primer[b]
Δ*nsrR*	TTTTTCCTTCCCCG AACTGA	ATATTGTCGCCCA GCACTTC	GGATTACGTGCGC TGATCTA	AAAGCGGTTGATT CTCTTCAA
Δ*hmp*	CCGAATCATTGTGC GATAACA	GCAAAATCGGTGA CGGTAAA	TCCCTTTACTGGTG GAAACG	CACGCCCAGATCC ACTAACT
Δ*katE*	TATTTGCCACGCAG CATCCA	TTGAGACTGCTGA CAAACGCAAA	AAAAACTCACCGG ACGTGAC	TCACCCATTCGGG AGTAGAG
Δ*katG*	ATCTCAACTATCGC ATCCGTGGA	CAGGGCAATGGCT AAGGTGTATTTA	CAACCGAGATGGG TCTGATT	CTCAACACCAACC ACACCAG
Δ*sdsN*	ATAGTAAACCGCA ACGCCCC	N/A	N/A[*]	TCGGGGCTGGACG CCATTTC
Δ*oxyR*	GTTAAAAGAGGTG CCGCTCC	N/A	TTGAGTACCTGGT GGCATTG	GAAATGGCCATCC ATTCTTG
Δ*rpoS*	CCATAACGACACA ATGCTGGTC	TATCTGGGGTTGT CGGTAGC	AATGAAGATGCGG AATTTGATG	ATATTCAGCCCCT GCGTTTG
Δ*fur*	GCCAGGGACTTGTG GTTTTC	N/A	CAATACCGCCCTA AAGAAAGC	GTTCATCTTCGCG GCAAT
Δ*fnr*	TGTGCCAGCTTGTT CACACTT	N/A	GATCCCGGAAAAG CGAATTA	AGGCAACGTTACG CGTATGA

[a] Following P1 transduction, proper chromosomal integration of the kanamycin resistance cassette (*kan*) was checked using a forward primer external to the gene on the chromosome and the following internal *kan* reverse primer: ATGATGGATACTTTCTCGGCAGGAG.

[b] Potential gene duplication was checked using forward and reverse primers internal to the gene.

[c] After removal of the *kan* cassette, proper scar size was confirmed with forward and reverse primers external to the gene on the chromosome.

[*] Due to the small size of *sdsN*, cPCR for Δ*sdsN* was performed only with the forward external primer and the reverse internal primer.

Table S2.2: qPCR primers

Target gene	Forward primer	Reverse primer
phzM	CGGCGAAGACTTCTACAGCTA	CAGGATGGCCTTGGTCAAT
gfp_{mut2}	GGTGATGTTAATGGGCACAA	GGCCATGGAACAGGTAGTTT

Table S2.3: Plasmid construction primers

Function	Forward primer	Reverse primer
Copy *hmpp-hmp* from wild-type genome for pWCKA02 construction	GCGCATCTCGAGGAACAGT ATAACCGAATCAT	GCGCGCCCTGCAGGTTAC AGCACCTTATGCGGGC
Copy $hmpp_{trunc}$-*hmp* from wild-type genome for pWCKA03 construction	GCGCGCCTCGAGTCTTTCT GAAAAACACCA	GCGCGCCCTGCAGGTTAC AGCACCTTATGCGGGC
Copy *nsrRp-nsrR* from wild-type genome for pWCKA04 construction	GCGCGCCTCGAGGTCGGGT AAGCCATTACG	GCGCGCCCTGCAGGTCAC TCCACCAGCAAT

Table S.2.4: Wanner knock-out primers

Function	Forward primer	Reverse primer
Copy *kan* from pKD4, with homology to the upstream and downstream of *sdsN*	CAAACTATCACATAAATAA GATTTATATATAATTTATAT TGTGTAGGCTGGAGCTGCT TC	ACCCGCCAGTTCCTCGAG AAGTTTCTGCTGCAATAA TAAGATGGGAATTAGCCA TGGTCC

References

1. Adolfsen, K.J. and M.P. Brynildsen, *A Kinetic Platform to Determine the Fate of Hydrogen Peroxide in Escherichia coli.* PLoS Comput Biol, 2015. **11**(11): p. e1004562.
2. Chou, W.K. and M.P. Brynildsen, *Loss of DksA leads to multi-faceted impairment of nitric oxide detoxification by Escherichia coli.* Free Radic Biol Med, 2019. **130**: p. 288-296.
3. Zaslaver, A., et al., *A comprehensive library of fluorescent transcriptional reporters for Escherichia coli.* Nat Methods, 2006. **3**(8): p. 623-8.
4. Cherepanov, P.P. and W. Wackernagel, *Gene disruption in Escherichia coli: Tc R and Km R cassettes with the option of Flp-catalyzed excision of the antibiotic-resistance determinant.* Gene, 1995. **158**: p. 9-14.
5. Datsenko, K.A. and B.L. Wanner, *One-step inactivation of chromosomal genes in Escherichia coli K-12 using PCR products.* PNAS, 2000. **97**(12): p. 6640-5.
6. Robinson, J.L. and M.P. Brynildsen, *An ensemble-guided approach identifies ClpP as a major regulator of transcript levels in nitric oxide-stressed Escherichia coli.* Metab Eng, 2015. **31**: p. 22-34.